

Application of Sensory Body Schemas to the Orientation Control of Hand-held Tactile Tonometer

Eniko T. Enikov and Phillip Vidinski

*Department of Aerospace and Mechanical Engineering, University of Arizona,
1130 N. Mountain Ave, Tucson, AZ 85721, U.S.A.*

Keywords: Spherical Parallel Mechanism, Artificial Neural Network, Body Schema, Cognitive Robotics.

Abstract: Body schemas are a biologically-inspired approach, emulating the plasticity of the animal brains, allowing efficient representation of non-linear mapping between the body configuration space, i.e. its generalized coordinates and the resulting sensory outputs. This paper describes the development of closed-loop control of spherical parallel mechanism based on self-learning body schemas. More specifically, we demonstrate how a complex parallel spherical manipulator in contact with a surface of irregular geometry can be driven to a configuration of balanced contact forces, i.e. aligned with respect to the irregular surface. The approach uses a pseudo-potential functions and a gradient-based maximum seeking algorithm to drive the manipulator to the desired position. It is demonstrated that a neural-gas type neural network, trained through Hebbian-type learning algorithm can learn a mapping between the manipulator's rotary degrees of freedom and the output contact forces. Numerical and experimental results are presented illustrating the performance of the control scheme. A motivating application of the proposed manipulator and its control algorithm is a hand-held eye tonometer based on tactile force measurements. The resulting controller has been shown to achieve 10 mN of force errors which are adequate for tactile tonometers.

1 INTRODUCTION

During the last ten years, we have seen an emergence of small low-cost devices, designed to perform some type of medical diagnostic function. Examples include a hand-held impedance plethysmograph for measuring heart rates variation (Kristiansen et al., 2005), various tonometers for eye pressure measurements at home (Doherty et al., 2012; Polyvas et al., 2013), and vagus nerve stimulators for management of headaches and other neurological conditions (Gaul et al., 2014). One novel application of hand-held devices is non-invasive measurement of eye pressure. Currently, the most trusted technique for measuring eye pressure is the Goldman applanation tonometry (GAT) (Davson, 1984). GAT has to be performed in a eye clinic due to the required anesthesia and sterilization. Efforts to develop more convenient devices for home use include tonometers such as Reichert Tono-Pen, a non-contact air-puff tonometer (Evans and Wishart, 1992), the rebound tonometer (I-Care and I-CareONE),(Fernandes et al., 2005) and t trans-palpebral (through the eyelid) Diaton tonometer. Tono-Pen is the hand-held version of the Gold-

mann tonometer and is also based on the Imbert-Fick law, thus requiring contact with the cornea. Reichert 7 uses an air jet, which applanates the eye, while rebound tonometers (I-Care and I-Care One) use an induction coil to magnetize a probe and launch it against the cornea. Diaton uses a similar principle, but in this case, the plunger falls on the eyelid due to gravity instead of induction coil (Doherty et al., 2011). This is the only trans-palpebral tonometer currently on the market, however it also requires the assistance of a trained professional aligning the device to the subject's eye. None of these existing devices have been approved for home use and therefore gathering continuous data from patients is not possible.

This paper presents the development of a novel positioning device, intended to achieve automatic alignment of hand-held tonometer with respect to an eyeball (soft sphere). In a prior work, we have investigated the forces arising from indentation of a human eye by an array of contact probes arranged asymmetrically (see Fig. 1). Differences between the forces measured by the central probe and peripheral forces is used to determine the stiffness and hence the eye pressure (Polyvas et al., 2013). The effectiveness and

accuracy of these devices is often determined by their placement and orientation with respect to the soft tissue of the human body. For example, the required accuracy of a hand-held tonometer placement should be within ± 3 degrees, in order to obtain a valid reading (Enikov et al., 2011). Consequently, successful development of such devices requires some type of mechanism for alignment of the device with respect to the soft tissue.

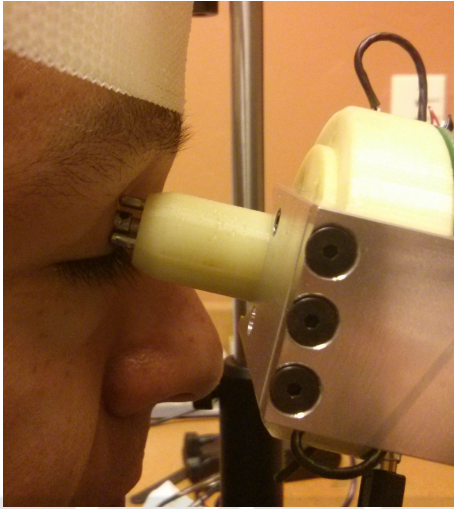


Figure 1: Tactile tonometer applied to a human.

One particular challenge is adjustment of the three peripheral force sensors with respect to the eye ball. Typically, an operator spends 2-5 minutes aligning the device to the test subject's eye. During this period, the user adjusts the orientation of the sensor and his eye gaze until the forces measured on three peripheral probes are within ϵ according to

$$|F_i - F_j| \leq \epsilon, i \neq j, \epsilon > 0. \quad (1)$$

Condition (1) ensures that the instrument is aligned with respect of the eye, however achieving such alignment is difficult. In order to assist the user in aligning the device, we propose a self-aligning tip, based on a spherical parallel mechanism (SPM). SPM-s allow rotations of the end-effector on a virtual sphere, centered at the tip of the device. Prior work on such devices include the development of the agile eye (Gosselin and Hamel, 1994), which is a camera orienting device. A large volume of subsequent studies have shown that this mechanism has large stiffness and rapid dynamic response (Wu and Zou, 2016). The proposed end effector is shown in Figure 2.

A total of nine revolute joints (three per kinematic chain) are used to constrain the tip to rotate about point P (spherical motion). In order to balance the contact forces, one has to solve an inverse kinematic

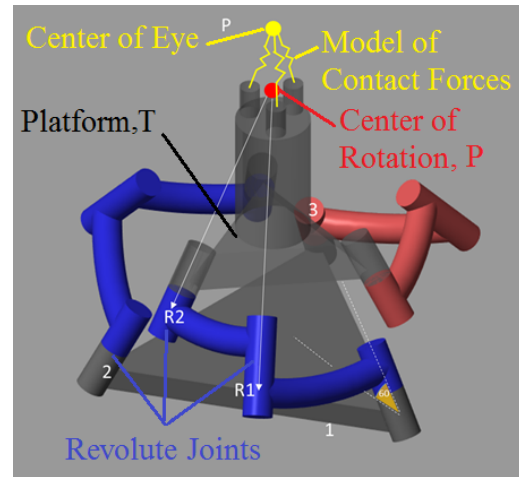


Figure 2: Spherical Parallel Mechanism: Axes of all cylindrical joints point towards the center of rotation. Cylindrical joints 1, 2, and 3 are driven by stepper motors resulting in 3-DOF motion of the triangular platform T.

problem relating the rotations of the tip to the rotations of the revolute joints (Gosselin and Hamel, 1994). This classical approach requires accurate modeling of the contact problem and solution of constraint equations in real time. In contrast, the approach taken here is based on self-learning robot, which uses bode schemas to learn the non-linear relationship between the angles of the input revolute joints and the resulting contact forces.

The pliability of body schemas and ability to operate in unknown environments is one of the main reasons a growing number of roboticists apply body schemas, i.e. motor, tactile, visual in the development of adaptable robots, capable of acquiring knowledge of themselves and their environment. Recent experiments in cognitive developmental robotics have demonstrated that using tactile and vision sensors, a robot could learn its body schema (image) through babbling in front of a camera and acquiring an "image" of its invisible face through Hebbian self-learning (Fuke et al., 2007).

In this paper we extend the computational approach introduced by Morasso (Morasso and Sanguineti, 1995) to create a link between the input angles of the revolute joints and the tactile sensor space. The trained network is then capable of representing a self-learned body schema allowing control of the end effector in a feed-forward mode. A unique feature of the approach is that the robot control task does not require the use of inverse kinematics. These features of the proposed control scheme are illustrated in the subsequent sections of this paper.

2 SELF-ORGANIZING BODY SCHEMA OF MAV-s

2.1 Classical 3-DOF Manipulator Model

The SPM is modelled using the coordinates of the unit vectors representing the axis of each joint (see Fig. 3). The vectors $u_i, i = 1, 2, 3$ are fixed in space and are represent the axis of rotation of the driving motors. Each of

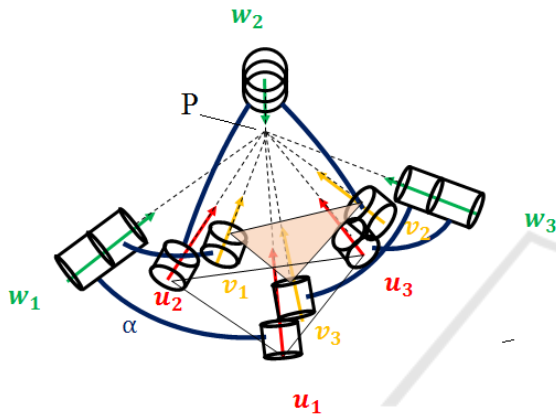


Figure 3: Unit-vectors of Revolute Joints.

these joints rotates through angles $\theta_i, i = 1, 2, 3$. The vectors $w_i, i = 1, 2, 3$ designate the directions of the intermediate revolute joints, and vectors $v_i, i = 1, 2, 3$ represent the directions of the distal joints attached to the end effector. Using standard matrix algebra, one can express the vectors v_i as trigonometric functions of the platform rotation angles Ω_x, Ω_y , and Ω_z , i.e. $w_i(\Omega_j), j = x, y, z$. Similarly, the intermediate vectors, w_i can be expressed as functions of the input angles θ_i , i.e. $v_i(\theta_i), i = 1, 2, 3$ (Gosselin and Lavoie, 1993). To obtain an input-output kinematic relationship, one uses the obvious constraint between the normal vectors

$$v_i(\Omega_j) \cdot w_i(\theta_i) = \cos(\alpha), i = 1, 2, 3, j = x, y, z \quad (2)$$

where α is the angle between the two vectors (see Fig. 4).

Equations (2) represent a non-linear transformation between input and output angles. Under a classical approach, its time derivatives result in the inverse Jacobian needed to relate the input angular velocities $\dot{\theta}_i$ to the platform angular velocities $\dot{\Omega}_j$. With the position of the end plate determined, one can use linear force-displacement relationships to determine the contact forces. An equivalent model was implemented in Matlab Simmechanics as a way of testing the neural network-based approach presented next.

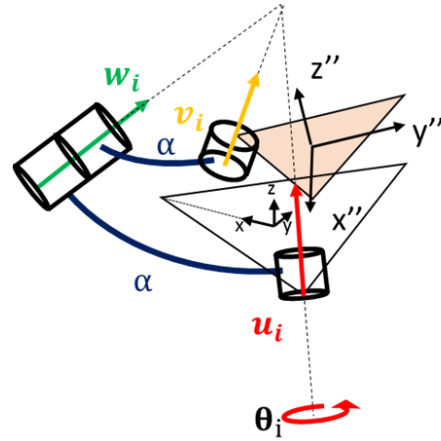


Figure 4: Angles Between Directional Unit-Vectors.

2.2 Body and Sensor Schemas

The use of body and sensor schemas is an alternative to the classical method described in the previous section. Rather than using an analytical model such as (2), a self-organizing body schema (So-BoS) can be used to link the manipulator's output (sensory) space \mathcal{S} with its input (configurational) space \mathcal{C} . A detailed review of applications of body schema-s in robotics can be found in (Hoffmann et al., 2010). As an extension of the approach of Morasso (Morasso and Sanguineti, 1995) and Stoychev (Stoychev, 2003), instead of vision data, the sensor space of the proposed SPM manipulator contains contact forces measured by the three peripheral probes $\mathbf{F} = (F_1, F_2, F_3)$. One essential advantage of So-BoS is the ability to model not only the transformation between input motor angles θ_i and the position of the end-effector, but also to predict the resulting forces. These forces are a function of the position of the hand-held unit with respect to the eye, i.e. an unknown error is introduced by the user.

Similar to conventional self-organizing neural network maps, a layer of neurons (processing units) is used to learn the mapping between the configuration space (generalized position of the robot) and the output of the tactile force sensors. Unlike other topologically ordered self-organizing maps such as the Kohonen map (Kohonen, 1982), the neurons in the present approach are initially disordered, i.e. forming a "neural gas" (Martinetz et al., 1991). The training process modifies the weights of each neuron until the network learns N body icons representing the CS -space. More specifically, denoting by $\mu = [\theta_1, \theta_2, \theta_3]$ the manipulator's input joint angles, and by $\beta = [F_1, F_2, F_3]$ the vector of contact sensor outputs, then for each body position i , the generalized co-

ordinates and associated sensors outputs will present an instance of these two vectors $\tilde{\mu}_i = [\tilde{\theta}_1^i, \tilde{\theta}_2^i, \tilde{\theta}_3^i] \in \mathcal{C}$ and $\tilde{\beta}_i = [\tilde{F}_1^i, \tilde{F}_2^i, \tilde{F}_3^i] \in \mathcal{S}$, respectively. The matched pairs $(\tilde{\beta}_i, \tilde{\mu}_i) \in \mathcal{CS}$ are referred to as body icons. The \mathcal{CS} space is approximated by a field of N neurons, each storing a learned body icon $(\tilde{\beta}_i, \tilde{\mu}_i), i = 1, \dots, N$. Associated with each neuron is an activation function, $U_i(\mu)$, which in this case is chosen to be the softmax function given by

$$U_i(\mu) = \frac{G(\|\mu - \tilde{\mu}_i\|)}{\sum_j G(\|\mu - \tilde{\mu}_j\|)},$$

where G is a Gaussian function with variance σ^2 . The normalization of $U_i(\mu)$ ensures that it has a maximum at $\mu = \tilde{\mu}_i$. The choice of σ determines the range of activation of neighboring neurons when computing the response of the network through

$$\mu^{approx} = \sum_j^N \tilde{\mu}_j U_j(\mu). \quad (3)$$

Similarly, the output of the sensory system is produced by

$$\beta^{approx}(\mu) = \sum_j^N \tilde{\beta}_j U_j(\mu). \quad (4)$$

The network training process is based on a competitive learning process, where the N neurons are presented with a large number of pseudo-random training vectors $\hat{\mu}_l, l = 1, \dots, I$. In the present example $N = 400$ and $I = 501$. For each training cycle, all training vectors $\hat{\mu}_l$ are presented to the network and the body icons are updated according to their respective learning laws

$$\Delta \tilde{\mu}_j = \eta_1 (\hat{\mu}_l - \tilde{\mu}_j) U_j(\hat{\mu}_l) \quad (5)$$

and

$$\Delta \tilde{\beta}_j(\mu) = \eta_2 (\beta - \tilde{\beta}_j) U_j(\hat{\mu}_l). \quad (6)$$

The parameters η_1 and η_2 are the learning rates for each law, respectively. The competitive learning process involves reduction of the learning rate as well as the range of activation specified by σ as the training proceeds. Through (4), the trained network represents a mapping between the manipulator's configuration space, \mathcal{C} and the resulting sensor space, \mathcal{S} . Therefore, it is an implicit calibration procedure.

Figure 10 presents the 501 training vectors (blue dots) and the learned body icons (green circles) upon training of $N = 400$ through $N_T = 10$ training cycles. In this example only two forces (F_1 and F_2) were used in the sensor space. The starting learning rates are $\eta_1 = \eta_2 = 0.9$, with variance $\sigma^2 = 1$. All three parameters were reduced linearly to $1/N_T$ of their starting values at the end of the last training epoch.

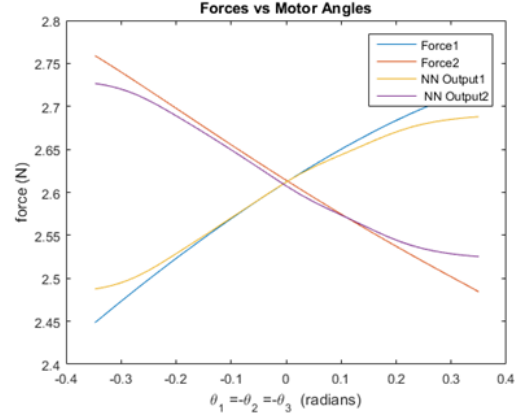


Figure 5: Training Force Data and Output of Trained Network.

One of the greatest benefits from the trained neural network and the associated mapping (4) is its ability to generate robot trajectories in the sensor space without explicitly computing its inverse Jacobian. This property of the body-schema based approach is illustrated in the next section.

3 TRAJECTORY PLANNING IN THE FORCE SPACE

Upon training, each processing unit has its preferred body icon $(\tilde{\beta}_i, \tilde{\mu}_i)$ allowing representation of the manipulator's sensory output through (4). In addition to the sensory output, the trained network can define additional functions over the configuration space or the sensory space. The present application requires path planning leading to a configuration where the forces are balanced according to (1). The advantage of the method is that the trained network does not require explicit inversion of the mapping between the manipulator's position and the output of the force sensors. Instead, the trajectory can be obtained through solution of an ordinary differential equation representing a gradient descent on a user-defined pseudo-potential field. More specifically, we use a pseudo-potential defined over the force space through

$$\xi(\mu) = \sum_j \tilde{\xi}_j(\hat{\beta}) U_j(\mu), \quad (7)$$

where $\tilde{\xi}_j$ are scalar weights for each processing unit. The potential weights can be selected such that the resulting pseudo-potential has an extrema (for example maximum) at the target landing location. Then a simple ordinary differential equation can be formulated that has a maximum- or minimum-seeking solution. Following the method of (Stoytchev, 2003), we

use a gradient ascend equation to drive the manipulator's input angular coordinates to the maximum of the pseudo-potential

$$\dot{\mu} = \gamma \nabla \xi(\mu) = \gamma \sum_{j=1}^N (\tilde{\mu}_j - \mu) \xi_j U_j(\mu). \quad (8)$$

The desired output, i.e. the force balance, can be specified by the choice of $\xi_j(\hat{\beta})$. The right-hand side of (8) provides the velocities of the input angles, θ_i , while its solution generates the trajectory.

To illustrate the approach, we have a two-dimensional example where the pseudo-potential becomes a surface over the coordinates θ_1 and θ_2 . The corresponding pseudo-potential is defined as

$$\xi(\mu) = A(F_1(\mu) - F_2(\mu))^4, \quad A = 10,000 \quad (9)$$

The actual weights are computed by evaluating (9) for each neuron j , i.e. $\xi_j = \xi_a(\tilde{\mu}_j)$. The corresponding pseudo-potential surface is shown in Figure 6 for $N=200$ neurons.

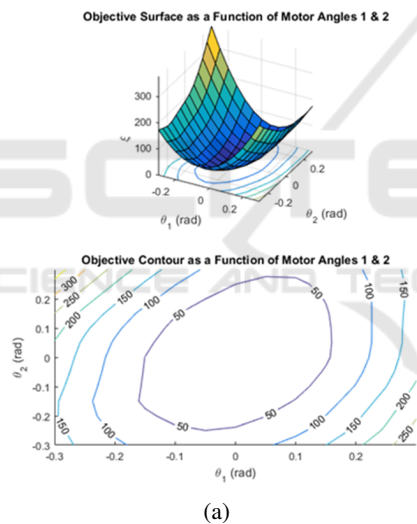


Figure 6: Pseudopotential surface ξ over the input angles θ_1 and θ_2 .

Solving equation (8) for a given pseudo-potential results in trajectories leading towards the target position. Figure 7 shows the convergence of the method for three initial conditions (IC-s) using the solution of (8) with $N=800$ neurons. The method was also tested experimentally as described in the next section.

4 EXPERIMENTAL VALIDATION

The validation of the proposed algorithm was carried out using a custom-designed experimental apparatus. A 3-DOF manipulator driven by three stepper motors

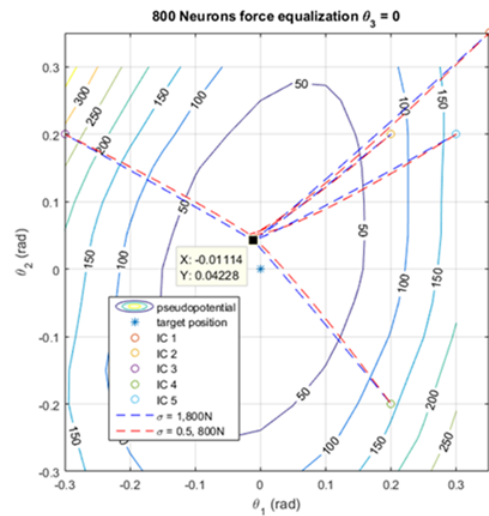


Figure 7: Simulated Trajectories For $\sigma = 1$ and $\sigma = 0.1$. Larger σ results in smoother maps and smaller steady-state errors.

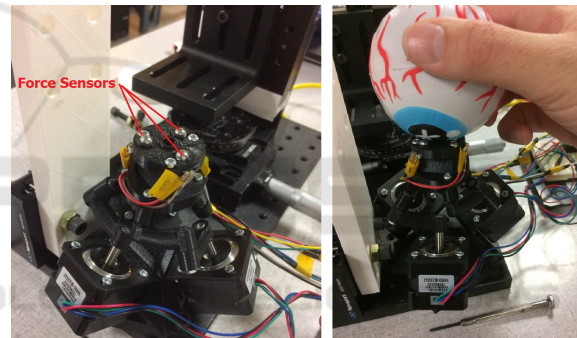


Figure 8: Experimental Apparatus.

was constructed as shown in Figure 8. A soft neoprene sphere was placed over the force sensors to emulate the presence of an "eye".

The experiment was carried out in two phases - training phase, where the SPM input angles θ_i were driven randomly in a range avoiding the kinematic singularities. The network was trained with the resulting force data and subsequently used in a closed-loop control configuration as illustrated in Figure 9.

The resulting controller is a form of feed-forward controller since the output forces are not fed back into the controller. Only position coordinates of the configuration space are needed, which are typically measured by the encoders of the motors.

Figure 10 shows the training data collected during 3.5 seconds of motion. One can notice that the force data is very irregular and noisy as is the case of manual positioning of the tonometer against the eye.

Upon turning on the controller, the two forces reach equal values within 3.5 - 4 seconds as illustrated in Figure 11.

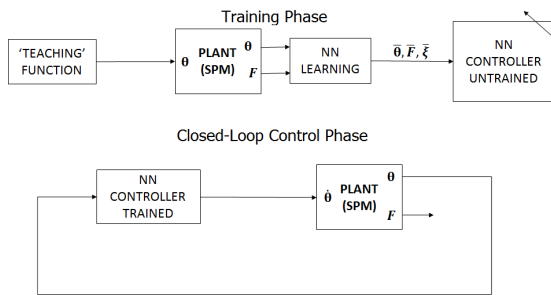


Figure 9: Training and Closed-Loop Control Phases of SPM.

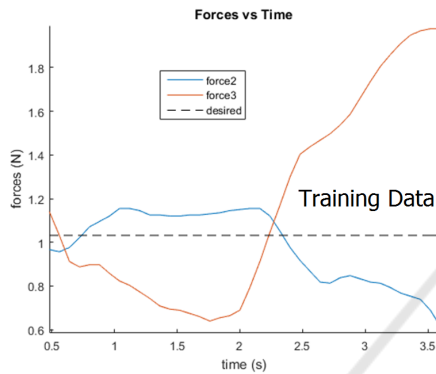


Figure 10: Experimental Results: Training Data.

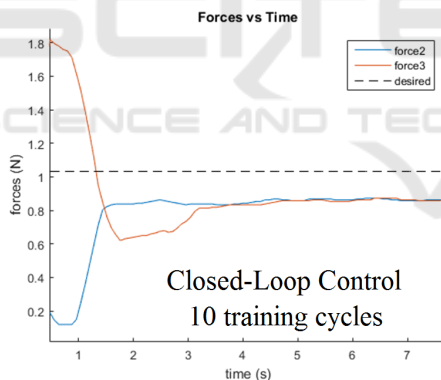


Figure 11: Experimental Results: Force Convergence.

In order to assess the sensitivity of the method with respect to the number of training cycles, i.e. ability to shorten the training period, the experiment was repeated with 5 and 7 training cycles, respectively. The force convergence for each case is shown in Figure 12. Clearly the performance degrades as the number of training cycles is decreased.

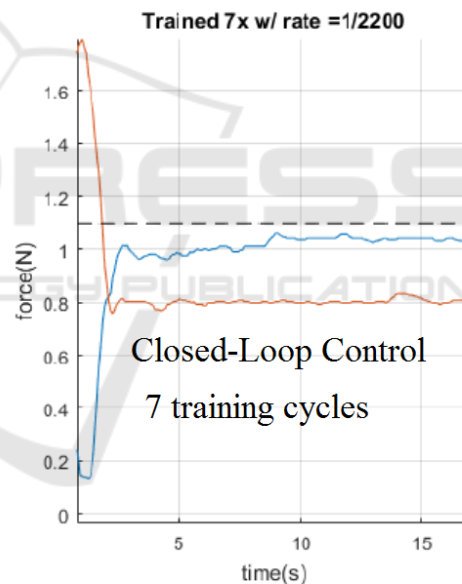
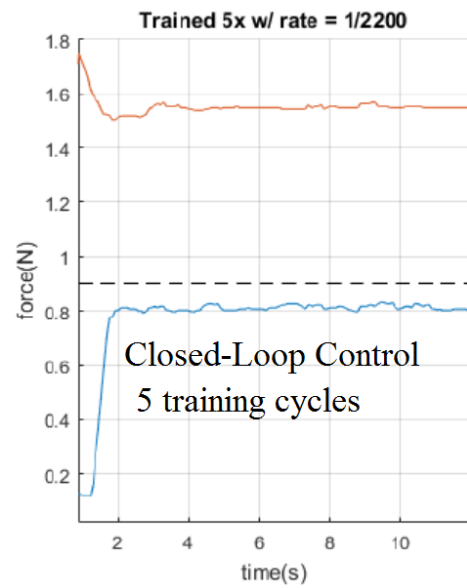


Figure 12: Experimental Results: Force Convergence using 5 (top) and 7 (bottom) training cycles.

5 SUMMARY AND CONCLUSIONS

The application of self-organizing artificial neural networks to the problem of controlling a manipulator in contact with a soft tissue has been described. It has been demonstrated that the neural network can fuse seamlessly the information gathered from multiple imperfect force sensors and significant noise. Upon

training period of 3.5 seconds, the network was able to drive the SPM manipulator to the desired balanced-force condition. The accuracy of the positioning is a function of the standard deviation (interaction distance) of neighboring neurons as well as the rate of descent. A total of 200 neurons trained over 10 cycles were used in the experiments, which resulted in fast training. A minimum of ten training cycles were required in order to produce robust controller, capable of balancing the forces within 10 mN. This force error corresponds to approximately 1 mmHg of error in tactile tonometry (Enikov et al., 2015). Therefore, the proposed approach appears suitable for implementation in a hand-held devices for diagnostic purposes.

ACKNOWLEDGMENTS

The authors acknowledge the partial support of NSF grant # 1446098.

REFERENCES

- Davson, H. (1984). In Davson, H., editor, *The Eye*, volume 1a. Academic Press, New York.
- Doherty, M., Carrim, Z., and O'Neill, D. (2012). Evaluation of the icare-one rebound tonometer as a self-measuring intraocular pressure device in normal subjects. *Clin Experiment Ophthalmol*, 40(4):171–175.
- Doherty, M. D., Carrim, Z. I., and O'Neill, D. P. (2011). Diaton tonometry: an assessment of validity and preference against goldmann tonometry. *Clinical & Experimental Ophthalmology*, pages no–no.
- Enikov, E., Polyvas, P., and M., M. (2011). Experimental and numerical analysis of ocular tactile tonometry. pages 1–5. IMECE2011, ASME International Mechanical Engineering Congress & Exposition.
- Enikov, E. T., Polyvas, P. P., Peyman, G., and Mccafferty, S. (2015). Tactile eye pressure measurement through the eyelid. In *ASME 2015 International Mechanical Engineering Congress and Exposition*, pages V003T03A022–V003T03A022. American Society of Mechanical Engineers.
- Evans, K. and Wishart, P. K. (1992). Intraocular pressure measurement in children using the keeler pulsair tonometer. *Ophthalmic and Physiological Optics*, 12(3):287–290.
- Fernandes, P., Daz-Rey, J. A., Queirs, A., Gonzalez-Mejome, J. M., and Jorge, J. (2005). Comparison of the i-care rebound tonometer with the goldmann tonometer in a normal population. *Ophthalmic and Physiological Optics*, 25(5):436–440.
- Fuke, S., Ogino, M., and Asada, M. (2007). Body image constructed from motor and tactile images with visual information. *International Journal of Humanoid Robotics*, 4(02):347–364.
- Gaul, C., Diener, H., Solbach, K., Silver, N., Straube, A., Magis, D., Reuter, U., Andersson, A., and Liebler, E. (2014). Ehmti-0364. non-invasive vagus nerve stimulation using gammacore® for prevention and acute treatment of chronic cluster headache: report from the randomized phase of the preva study. *The journal of headache and pain*, 15(1):17.
- Gosselin, C. M. and Hamel, J.-F. (1994). The agile eye: a high-performance three-degree-of-freedom camera-orienting device. In *Robotics and Automation, 1994. Proceedings., 1994 IEEE International Conference on*, pages 781–786. IEEE.
- Gosselin, C. M. and Lavoie, E. (1993). On the kinematic design of spherical three-degree-of-freedom parallel manipulators. *The International Journal of Robotics Research*, 12(4):394–402.
- Hoffmann, M., Marques, H. G., Hernandez Arieta, A., Sumioka, H., Lungarella, M., and Pfeifer, R. (2010). Body schema in robotics: a review. *Autonomous Mental Development, IEEE Transactions on*, 2(4):304–324.
- Kohonen, T. (1982). Self-organized formation of topologically correct feature maps. *Biological cybernetics*, 43(1):59–69.
- Kristiansen, N. K., Fleischer, J., Jensen, M., Andersen, K. S., and Nygaard, H. (2005). Design and evaluation of a handheld impedance plethysmograph for measuring heart rate variability. *Medical and Biological Engineering and Computing*, 43(4):516–521.
- Martinetz, T., Schulten, K., et al. (1991). *A "neural-gas" network learns topologies*. University of Illinois at Urbana-Champaign.
- Morasso, P. and Sanguineti, V. (1995). Self-organizing body schema for motor planning. *Journal of Motor Behavior*, 27(1):52–66.
- Polyvas, P. P., Peyman, G., and Enikov, E. T. (2013). Transscleral tactile tonometry: An instrumented approach. *Medical engineering & physics*, 35(7):937–943.
- Stoytchev, A. (2003). Computational model for an extendable robot body schema.
- Wu, G. and Zou, P. (2016). Comparison of 3-dof asymmetrical spherical parallel manipulators with respect to motion/force transmission and stiffness. *Mechanism and Machine Theory*, 105:369–387.